J. Fluid Mech. (1993), *vol.* 252, *pp.* 357–382

Similarities in the structure of swirling and buoyancy-driven flows

By P. A. DAVIDSON

Department of Mechanical Engineering, Imperial College, Exhibition Road, London SW7 2BX, UK

(Received 4 August 1992 and in revised form 3 February 1993)

We look at two classes of contained flow: swirling flow and buoyancy-driven flow. We note that the strong links between these arise from the way in which vorticity is generated and propagated within each. We take advantage of this shared behaviour to investigate the structure of steady-state solutions of the governing equations. First, we look at flows with a small but finite viscosity. Here we find that, Batchelor regions apart, the steady state for each type of flow must consist of a quiescent stratified core, bounded by high-speed wall jets. (In the case of swirling flow, this is a radial stratification of angular momentum.) We then give a general, if approximate, method for finding these steady-state flow fields. This employs a momentum-integral technique for handling the boundary layers. The resulting predictions compare favourably with numerical experiments. Finally, we address the problem of inviscid steady states, where there is a well-known class of steady solutions, but where the question of the stability of these solutions remains unresolved. Starting with swirling flow, we use an energy minimization technique to show that stable solutions of arbitrary net azimuthal vorticity do indeed exist. However, the analogy with buoyancy-driven flow suggests that these solutions are all of a degenerate, stratified form. If this is so, then the energy minimization technique, which conserves vortical invariants, may mimic the stratification of temperature or angular momentum in a turbulent flow.

1. Introduction

In this paper, we consider two distinct classes of motion: swirling flow and buoyancy-driven flow. Individually, each of these has been studied extensively, and a number of quite profound properties have emerged. Both may sustain internal wave motion, and both have a predisposition towards two-dimensionality. In the case of swirling flow, this manifests itself in the existence of Taylor–Proudman columns. The qualitative analogy between the two classes of flow has long been recognized, going back at least as far as Rayleigh's studies of centrifugal instability.

We are interested here in axisymmetric, contained flows. There is a considerable body of experimental evidence to suggest that, in the steady state, such flows tend to a state of stratification throughout most of the flow field. That is, in a swirling flow, the azimuthal velocity, u_θ, is a function only of the radial coordinate, r, while the temperature in a buoyancy-driven flow is a function only of the vertical position, z. (See Davidson 1992 for examples of the former, and Elder 1965 and Vives & Perry 1989 for examples of the latter.) However, there are many notable flows where this is not the case. Perhaps the most important exceptions are the Batchelor-like flows, where temperature, vorticity and angular momentum are all uniform (see Batchelor 1956). In

fact, there are even flows that appear to be neither stratified nor of the Batchelor type, but have a more complex form.

In this paper, we address two distinct, but related questions. Firstly, what is the formal nature of the analogy between swirling and buoyancy-driven flows, and can we use this to extend our knowledge of either? Secondly, under exactly what conditions will stratification of these flows occur, and can we use this knowledge to give an approximate solution for the flow field?

We start, in §2, by examining the mechanisms by which vorticity is generated and propagated in swirling and buoyant fluids. It turns out that the mechanisms are very similar, and that this underpins the more general links between the two topics. In §3, we illustrate these links by reviewing briefly the established analogies between swirling and buoyant flows. In particular, we look at thermal plumes and internal waves, and their counterparts in rotating fluids.

We turn next to the main focus of the paper, which is the structure of steady-state flows. Here we are interested in flows with a high Reynolds number and with closed streamlines. The fluid is taken as (almost) incompressible, with the Boussinesq approximation being used for the buoyancy force.

We start by examining steady-state flows with a small but finite viscosity. We show that, Batchelor regions apart, any steady state must consist of an inviscid, quiescent, stratified core, bounded by high-speed wall jets. The stratification is of angular momentum in the case of swirling flow (Taylor–Proudman theorem), and of temperature in the case of buoyancy-driven flow. In each case, all of the streamlines pass through both the boundary layer and the core. In addition, stratification of the core represents a minimum energy state.

Having established the general structure of these steady states, we go on to develop approximate methods for predicting the temperature and velocity fields. Following Greenspan (1968), the wall jets are handled using the momentum-integral technique, and the core and wall-jet flows are linked via continuity of mass. We illustrate this method with two particular examples: forced swirl in a cone, and buoyancy-driven flow in a cylinder. In each case, the predictions are compared with numerical experiments.

Finally, we address the question of inviscid steady states. Here we use the energy minimization technique of Vallis, Carnevale & Young (1989) to examine the stability of a well-known class of steady solutions. However, as Batchelor (1956) pointed out, such flows, if they exist, will not last for long. In reality, diffusion between closed streamlines will eventually eradicate any gradients in temperature, angular momentum or vorticity. Consequently, one must be very cautious in attributing physical significance to these flows.

We aim to achieve two goals with this paper. One is to show that there is a strong commonality between swirling and buoyancy-driven flows, and that given a solution of one type, we can (often) construct a flow of the other. Secondly, we aim to show that steady-state solutions of these flows (at high Reynolds numbers) are inevitably stratified, and we can use this knowledge to obtain approximate solutions for the flow fields.

2. The governing equations of motion

We shall restrict ourselves to axisymmetric flows, and adopt a cylindrical polar coordinate system (r, θ, z), with z pointing vertically downward. It is useful to separate the velocity $\boldsymbol{u}$ and vorticity $\boldsymbol{\omega}$ into azimuthal (θ) and poloidal (r, z) components.

Consider first a swirling, recirculating flow. The velocity field can be written in the form

$$\boldsymbol{u} = \boldsymbol{u}_p + \boldsymbol{u}_\theta = \boldsymbol{\nabla} \times [(\psi/r)\,\hat{\boldsymbol{e}}_\theta] + (\Gamma/r)\,\hat{\boldsymbol{e}}_\theta. \tag{1}$$

Here ψ is the Stokes streamfunction and Γ is the angular momentum, $u_\theta r$. The streamfunction is related to the vorticity component, ω_θ, by the operator ∇^2_*, defined by

$$-r\omega_\theta = \frac{\partial^2 \psi}{\partial z^2} + r\frac{\partial}{\partial r}\left(\frac{1}{r}\frac{\partial \psi}{\partial r}\right) = \nabla^2_* \psi. \tag{2}$$

Next, the azimuthal and poloidal components of the Navier–Stokes equations can be reduced to transport equations for Γ and ω_θ. If ν is the viscosity, these are,

$$\mathrm{D}\Gamma/\mathrm{D}t = \nu \nabla^2_* \Gamma, \tag{3}$$

$$\frac{\mathrm{D}}{\mathrm{D}t}\left(\frac{\omega_\theta}{r}\right) = \nu\left\{\nabla^2\left(\frac{\omega_\theta}{r}\right) + \frac{2}{r}\frac{\partial}{\partial r}\left(\frac{\omega_\theta}{r}\right)\right\} + \frac{\partial}{\partial z}\left(\frac{\Gamma^2}{r^4}\right). \tag{4}$$

Between them, the two scalars Γ and ω_θ completely describe the instantaneous state of the flow field.

Now consider the analogous, two-dimensional, buoyancy-driven flow. This consists of a poloidal velocity field $\boldsymbol{u}_p(r, z)$, in conjunction with a temperature field $T(r, z)$. We shall use the Boussinesq approximation, in which $\boldsymbol{u}_p$ remains solenoidal. In this case, the equation of motion is

$$\frac{\mathrm{D}\boldsymbol{u}}{\mathrm{D}t} = -\boldsymbol{\nabla}(P/\rho) - g\beta T \hat{\boldsymbol{e}}_z + \nu \nabla^2 \boldsymbol{u}, \tag{5}$$

where β is the expansion coefficient,

$$\beta = -\frac{1}{\rho}\frac{\mathrm{d}\rho}{\mathrm{d}T}.$$

As with the swirling flow, we may write (5) as a transport equation for ω_θ. If α is the thermal diffusivity, we have two governing equations:

$$\mathrm{D}T/\mathrm{D}t = \alpha \nabla^2 T, \tag{6}$$

$$\frac{\mathrm{D}}{\mathrm{D}t}\left(\frac{\omega_\theta}{r}\right) = \nu\left\{\nabla^2\left(\frac{\omega_\theta}{r}\right) + \frac{2}{r}\frac{\partial}{\partial r}\left(\frac{\omega_\theta}{r}\right)\right\} + \frac{g\beta}{r}\frac{\partial T}{\partial r}. \tag{7}$$

There is a similarity in the structure of equations (6) and (7), and (3) and (4). In the buoyancy-driven flow, the source of recirculation is a radial temperature gradient (Bjerkne's theorem), while for a centrifugal flow, it is the axial gradient in swirl. In both cases, there is a mutual interaction between the recirculation, $\boldsymbol{u}_p$, and Γ or T.

The source term on the right-hand side of (4) may be rewritten in the form $\boldsymbol{\nabla} \times (\boldsymbol{u}_\theta \times \boldsymbol{\omega}_p)$, showing that the physical origin of this term is a spiralling of the poloidal vortex lines by $\boldsymbol{u}_\theta$. That is, any axial gradient in Γ causes it to corkscrew its own vortex lines, sweeping out a component of ω_θ (see Davidson 1989). The source term on the right-hand side of (7) is physically more obvious. Any radially orientated element of fluid which is hotter at its outer radius than its inner radius will experience a net torque, rotating the element about a horizontal axis.

There are a number of instances where we will choose to neglect diffusion, and in this case the governing equations take particularly simple forms:

swirling flow

$$D\Gamma/Dt = 0, \tag{8}$$

$$\frac{D}{Dt}\left(\frac{\omega_\theta}{r}\right) = \nabla\cdot\left[\frac{\Gamma^2}{r^4}\hat{\boldsymbol{e}}_z\right]; \tag{9}$$

buoyancy-driven flow

$$DT/Dt = 0, \tag{10}$$

$$\frac{D}{Dt}\left(\frac{\omega_\theta}{r}\right) = \nabla\cdot\left[g\beta\frac{T}{r}\hat{\boldsymbol{e}}_r\right]. \tag{11}$$

Note that, if we replace $g\hat{\boldsymbol{e}}_z$ by a *fictitious radial gravity*, $gr^{-3}\hat{\boldsymbol{e}}_r$, then the two sets of equations become identical. That is, there is an exact correspondence between swirling flow and an (unphysical) r^{-3} radial gravity. This, in turn, suggests a qualitative analogy between physical ($g\hat{\boldsymbol{e}}_z$-driven) buoyancy and swirl. In fact, it is readily shown that equations (8) and (9), and (10) and (11) are identical provided we confine attention to a narrow annulus (surrounding $r = r_0$) within which gradients in r are much greater than the azimuthal curvature, $1/r_0$. This was noted by Pumir & Siggia (1992), and becomes evident if we rewrite (10) and (11) in terms of the variables $\bar{\Gamma}^2 = -r_0^3 g\beta T$, $y = r - r_0$, $\bar{\psi} = -\psi/r_0$, and $\bar{\omega} = -\omega_\theta$. For $y \ll r_0$ and $1/r_0 \ll \partial/\partial y$, we obtain

$$\frac{\partial\bar{\Gamma}}{\partial t} + \frac{\partial(\bar{\psi},\bar{\Gamma})}{\partial(z,y)} = 0; \quad \frac{\partial\bar{\omega}}{\partial t} + \frac{\partial(\bar{\psi},\bar{\omega})}{\partial(z,y)} = \frac{1}{r_0^3}\frac{\partial\bar{\Gamma}^2}{\partial y},$$

while the corresponding equations for swirling flow are

$$\frac{\partial\Gamma}{\partial t} + \frac{\partial(\psi^*,\Gamma)}{\partial(y,z)} = 0; \quad \frac{\partial\omega_\theta}{\partial t} + \frac{\partial(\psi^*,\omega_\theta)}{\partial(y,z)} = \frac{1}{r_0^3}\frac{\partial\Gamma^2}{\partial z},$$

where $\psi^* = \psi/r_0$. Reversing y and z in either set of equations gives the desired result. Thus the qualitative analogy between swirl and buoyancy becomes exact in cases where azimuthal curvature is relatively small. The same is also true, in cases where $\alpha = \nu$, of the diffusive equations (3), (4), (6) and (7).

This similarity in structure has important consequences for both steady and unsteady flows. For example, it is well known that (8) and (9) admit two classes of steady solution (Batchelor 1967). The first is the degenerate case $\Gamma = \Gamma(r)$, $\psi = 0$. The second comes from rewriting the steady-state version of (9) in the form

$$\frac{D}{Dt}\left(\frac{\omega_\theta}{r} - \frac{\Gamma\Gamma'(\psi)}{r^2}\right) = 0,$$

from which

$$\Gamma = \Gamma(\psi),$$

$$\nabla_*^2\psi = -\Gamma\Gamma'(\psi) + H'(\psi)\,r^2.$$

Here H is an arbitrary function of ψ. Given $H(\psi)$ and $\Gamma(\psi)$, we may solve this equation for ψ. It is readily verified that the equivalent steady-state, buoyancy-driven flows are of the form

$$T = T(\psi),$$

$$\nabla_*^2\psi = -g\beta T'(\psi)\,zr^2 + H'(\psi)\,r^2,$$

where, once again, H is an arbitrary function. This class of solution is, perhaps, less well known. We can even combine the results above, so that, in the presence of both swirl and buoyancy, the streamfunction satisfies

$$\nabla_*^2\psi = -g\beta T'(\psi)\,zr^2 - \Gamma\Gamma'(\psi) + H'(\psi)\,r^2.$$

The similarity also carries over into unsteady flows. For unsteady, swirling flow, Davidson (1989) showed that there is a class of integral invariants of the motion. These are associated with any material volume, V_Γ, which is bounded by the toroidal surface, $\Gamma =$ constant. The existence of the invariants can be most readily demonstrated by rearranging (8) and (9) in the form

$$\frac{\mathrm{D}}{\mathrm{D}t}\left\{\frac{\omega_\theta}{r}g(\Gamma)+f(\Gamma)\right\} = \nabla\cdot\left\{\frac{2}{r^4}\int_0^\Gamma g(\Gamma)\,\Gamma\,\mathrm{d}\Gamma\hat{\boldsymbol{e}}_z\right\},$$

where g and f are arbitrary functions of Γ. Integrating this over V_Γ, invoking the divergence theorem, and noting that the integral on the right-hand side is constant over the surface, we find invariant integrals of the form

$$I = \int_{V_\Gamma}\left\{\frac{\omega_\theta}{r}g(\Gamma)+f(\Gamma)\right\}\mathrm{d}V.$$

The simplest of these integrals is the 'signature function', $V_I(\Gamma)$. The equivalent result for diffusionless, buoyancy-driven flow is

$$\frac{\mathrm{D}}{\mathrm{D}t}\int_{V_T}\left\{\frac{\omega_\theta}{r}g(T)+f(T)\right\}\mathrm{d}V = 0,$$

where V_T is any material volume bounded by an isothermal surface. Clearly, although the analogy is not exact, there is a substantial similarity in the structure of swirling and buoyant flows.

Although we are interested, primarily, in steady flows, we may best illustrate this structural similarity with reference to some well-known unsteady flows. There are (at least) two striking analogies which are established in the literature, and we will touch briefly on each of them. These are vortex rings and internal waves. The second of these will prove to be important in our discussion of inviscid steady states in §7.

3. Review of analogous swirling and buoyancy-driven flows

Two of the most striking phenomena associated with unsteady buoyant flows are: (*a*) the formation of thermal plumes from isolated sources; and (*b*) the propagation of internal gravity waves in a stratified fluid. The arguments of §2 suggest that corresponding swirling flows should exist, and this is indeed known to be the case. We shall review these flows briefly, largely to emphasize the links established in §2. However, these examples also serve to illustrate the mechanisms by which vorticity is generated and propagated within swirling and buoyant flows. These mechanisms are essentially the same for each, and it is this similarity which underpins the more general links between the two subjects. We start with thermal plumes.

Suppose we release a spherical blob of light fluid in an otherwise quiescent, heavy liquid. The blob will, of course, rise. However, after a short time its shape evolves into a mushroom-like structure, with a well-defined cap and an indented base. This structure is illustrated by the impulsively generated thermal plumes shown in Turner (1973) and Van Dyke (1982). Pumir & Siggia (1992) used the qualitative analogy between swirl and buoyancy to argue that a localized ring of swirl will behave in a similar way, organizing itself into a form of thermal plume. A finite-difference computation of an inviscid, axisymmetric flow supported this assertion. In fact, such flows have been realized in the laboratory by, for example, the Japan Society of Mechanical Engineers (1988). If a cylinder is impulsively rotated in a quiescent fluid, an unstable swirling boundary layer builds up on its outer surface. Ring-shaped

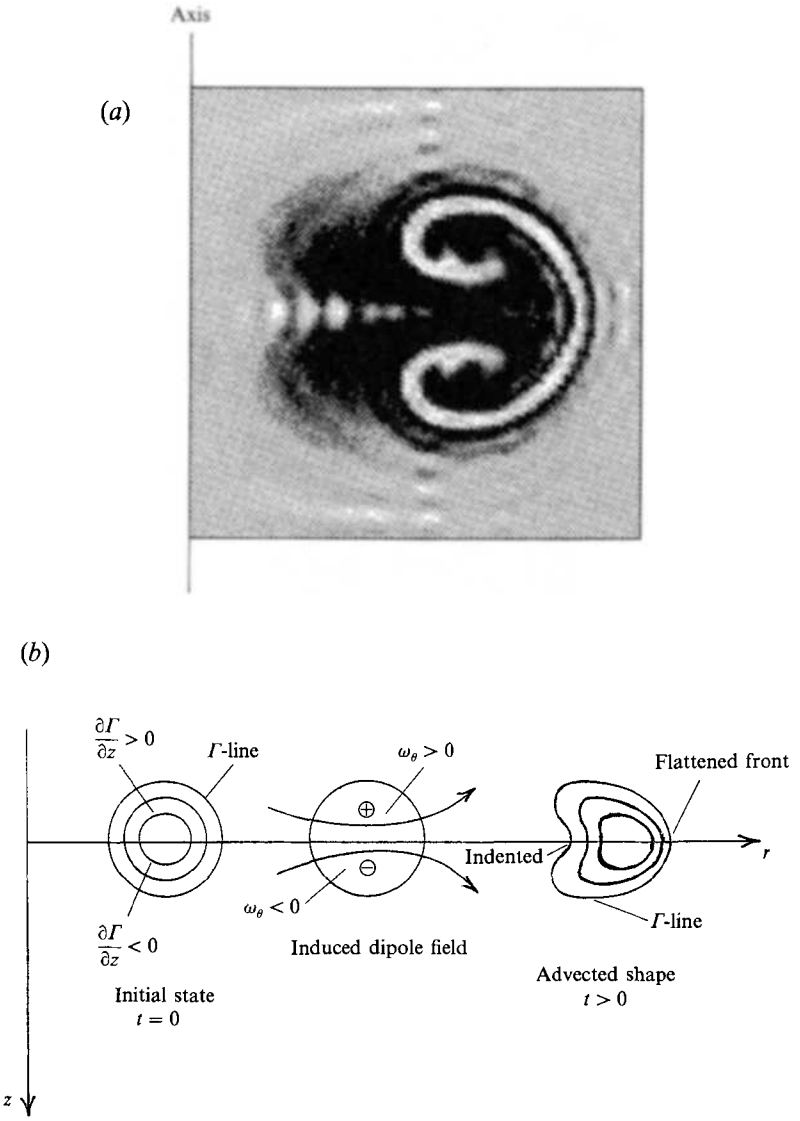

FIGURE 1. Swirling vortex ring. (*a*) A hoop of swirling fluid is released at $t = 0$. The hoop centrifuges itself radially outward, developing the mushroom-like structure of a thermal plume. (The contours are of constant angular momentum.) (*b*) Mechanism of propagation. Above the plane $z = 0$ we have $\partial\Gamma/\partial z > 0$, and so ω_θ is positive. Below the plane $z = 0$ we have $\partial\Gamma/\partial z < 0$, and so ω_θ is negative. The resulting dipole field propagates the ring radially outward.

vortices of swirling fluid are shed from this boundary layer, and these propagate radially outward with the characteristic mushroom-like structure of a thermal plume.

Pumir & Siggia were, however, less concerned with the overall structure of these rings than with the details of the propagating front. Their aim was to show that, if the flow is inviscid, a singularity in vorticity develops at the front within a finite time. Indeed, they exploited the analogy with buoyancy, which becomes exact once a singularity starts to evolve, to replace the axisymmetric Euler equations at the front by the two-dimensional Boussinesq equations, the latter being simpler to compute.

An example of such a swirling vortex ring is shown in figure 1(*a*), where the contours correspond to lines of constant angular momentum. The initial condition

consisted of $\boldsymbol{u}_p = 0$ and of Γ confined to a circular hoop, and we have computed the subsequent evolution of the ring using a spectral-based code. We can interpret the development of the mushroom-like structure with the aid of (8) and (9), in conjunction with figure 1(*b*). At $t = 0$, the cross-section of the hoop consists of concentric circular Γ-lines. The initial axial gradients in Γ give rise, via (9), to a dipole field, $\boldsymbol{u}_p$, as shown. This then advects the hoop radially outward. However, the key to explaining the change in shape of the ring lies in the time derivative in (9). This ensures that the magnitude of ω_θ/r always lags behind the distribution of Γ which caused it. Thus, while the dipole field $\boldsymbol{u}_p$ is still growing, the hoop edges radially outward, so that the inner radius of the vortex ring experiences a greater velocity than the outer radius, and the inside surface of the hoop becomes indented. In addition, the straining motion at the front of the hoop flattens its outer surface and increases the local radial gradient in Γ.

Pumir & Siggia were concerned particularly with the growth of vorticity near the front. However, it is also possible to calculate the global rise in ω_θ, and use this to estimate the rate of propagation of the hoop. Let κ be the volume integral of ω_θ/r in the top half of the hoop, then, from (9),

$$\frac{\mathrm{d}\kappa}{\mathrm{d}t} = 2\pi \int_{r_i}^{r_o} \frac{\Gamma_*^2}{r^3} \mathrm{d}r,$$

where r_i is the inner hoop radius, r_o is the outer hoop radius, and Γ_* is the angular momentum distribution along the r-axis. Now we know that a pair of two-dimensional point vortices, $+\kappa$ and $-\kappa$, separated by a distance d, propagate at the constant speed of $\kappa/2\pi d$. Consequently, if we ignore azimuthal curvature, the expression above gives an estimate of the radial acceleration of the hoop. Of course, this expression remains valid only for as long as viscosity can be ignored. One striking feature of this inviscid analysis is that the strength of the azimuthal vorticity, κ, increases monotonically. This is one manifestation of the fact that kinetic energy is continuously transferred from the swirling flow to the recirculation, at the rate

$$\dot{E}_p(t) = -\dot{E}_\theta(t) = -\frac{\mathrm{d}}{\mathrm{d}t} \int_V \tfrac{1}{2} u_\theta^2 \, \mathrm{d}V = \int_V \frac{\Gamma^2}{r^3} u_r \, \mathrm{d}V.$$

We may apply the same analysis, with little modification, to our rising blob of hot fluid. Suppose that the blob is initially spherical, and has a uniform temperature T (relative to the ambient). Let α and ν be small so that we may (initially) neglect diffusion. If κ is the volume integral of ω_θ/r for the blob, (11) gives us

$$\frac{\mathrm{d}\kappa}{\mathrm{d}t} = -2\pi g \beta T l.$$

Here l is the instantaneous height of the blob. As before, vorticity and kinetic energy increase monotonically, convecting the hot fluid upwards.

This simple example illustrates the proposition that, for a given buoyancy-driven flow, we are often able to construct an analogous swirling flow (and vice versa). The common link is the manner in which vorticity, ω_θ, is generated and propagated. Moreover, this correspondence is not limited to diffusionless flows, as illustrated by the exact analogy between an Ekman layer and the buoyancy layers generated on an inclined plate immersed in a stratified ($\nu = \alpha$) fluid (see Turner 1973). However, perhaps the best known and most striking example of the analogy is inviscid, internal wave motion. We will touch on this topic, partially because it plays an important role in §7, and partially because it leads naturally to a discussion of minimum energy states.

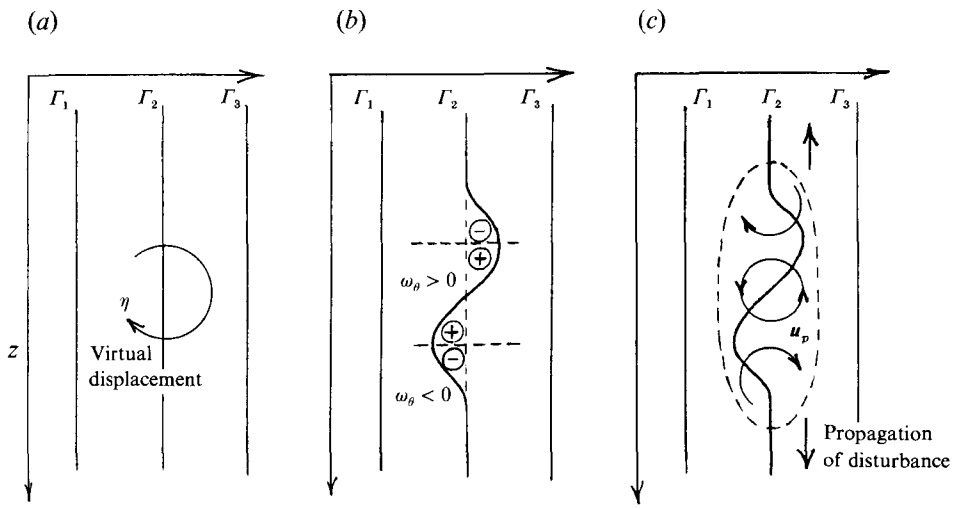

FIGURE 2. Propagation of a disturbance in a swirling flow. The induced recirculation propagates the disturbance along the Γ-line. This is an inertial wave. (*a*) Box flow, (*b*) generation of vorticity, (*c*) wave propagation.

The fact that stratified fluids can support internal gravity waves suggests that a swirling flow should also support internal waves. These are, of course, inertial waves. Consider a steady (base) flow, in which $\Gamma = \Gamma_0(r)$, $\boldsymbol{u}_p = 0$, and $\Gamma_0'(r) > 0$. Suppose that, at $t = 0$, we locally perturb this base flow by a virtual displacement, $\boldsymbol{\eta}$, as shown in figure 2(*a*). The resulting gradients in Γ give rise, via (9), to a recirculation as shown in figure 2(*c*). This causes the amplitude of the initial disturbance to diminish, while the disturbance itself propagates out along the Γ-line. However, if it were not for the time derivative on the left-hand side of (9), the disturbance would decay without oscillation. This time derivative ensures that the magnitude of ω_θ will lag behind that of $\partial\Gamma/\partial z$. Consequently, the diminishing amplitude of the disturbance will overshoot, flexing the Γ-line in the opposite direction. The net result is a wave motion, propagating energy out along the Γ-line.

The analogous gravity wave is considerably more familiar. The mechanism of wave propagation is precisely as before, with isotherms replacing Γ-lines, and r and z reversing roles. The equivalent base state is a quiescent, stratified fluid $T = T_0(z)$. (Stability requires $T_0'(z) < 0$.)

For each of these waves, the governing equation for small-amplitude disturbances may be found by linearizing (8)–(11) about their base states. In swirling flows, for example, the well-known linearized equation is

$$\frac{\partial^2}{\partial t^2}(\nabla_*^2 \psi) + \Phi(r)\frac{\partial^2 \psi}{\partial z^2} = 0, \tag{12}$$

where Φ is Rayleigh's discriminant (the square of the limiting wave frequency)

$$\Phi(r) = \frac{1}{r^3}\frac{\mathrm{d}\Gamma_0^2}{\mathrm{d}r}. \tag{13}$$

To obtain the equivalent equation for gravity waves, we exchange the gradients in r and z, and replace $\Phi^{\frac{1}{2}}$ by the Väisälä–Brunt frequency, N, defined by, $N^2 = -g\beta T_0'(z)$. Of course, as Rayleigh noted, Φ and N^2 play analogous roles in determining the stability

of the two systems (see Drazin & Reid 1981 and Vladimirov 1985). In fact, Φ is a direct measure of the increase in the kinetic energy of a swirling flow when two elements of the fluid at different radii are exchanged, while N^2 is a measure of the increase in the potential energy of a stratified fluid when fluid elements at different elevations are exchanged. This analogy has been the basis of attempts to relate changes in the structure of turbulence induced by density stratification to changes induced by streamline curvature (see Townsend 1976). We will return to (12) during our discussion of inviscid steady states.

The ability of the stratified flows $\Gamma_0(r)$ and $T_0(z)$ to dispatch disturbances to the far field gives them a certain robustness. This stability is a manifestation of the fact that these base flows represent minimum-energy states. To illustrate this, consider an inviscid unsteady swirling recirculating flow. It is shown in the Appendix that, if we divide the total kinetic energy into azimuthal and poloidal components, E_θ and E_p, then E_θ is bounded from below by

$$E_\theta = \int_V \tfrac{1}{2} u_\theta^2 \, \mathrm{d}V \geqslant \left\{ \int \Gamma \, \mathrm{d}V \right\}^2 \Big/ 2 \int r^2 \, \mathrm{d}V. \tag{14}$$

Moreover, the flow $u_\theta = \Omega r$, where Ω is independent of position, represents an absolute minimum in E_θ, while the flow $u_\theta = \Omega(r)\, r$, represents a local minimum in E_θ, provided Rayleigh's discriminant is positive. (This lower bound on E_θ will prove to be important in our discussion of inviscid steady states.) These results have an obvious counterpart in buoyant fluids, corresponding to stratification of T.

Intuitively, one would expect these minimum-energy states to play a central role in steady-state solutions of the equations of motion. We shall see that this is indeed the case. We start by addressing the problem of steady flows with a small but finite viscosity. Later, we look at inviscid steady states. In both cases, we are interested in contained flows, where the streamlines are closed.

4. Steady-state solutions for a small but finite viscosity

We start our discussion of high-Reynolds-number flows by looking at a swirling fluid. There are at least two ways in which viscosity can influence a swirling flow. One occurs when there is swirl on the boundary, and the other arises from internal diffusion. Consider first the case where $\Gamma = \Gamma_0(r)$. Then von Kármán boundary layers will form on all the surfaces that are not parallel to z. These boundary layers will entrain or detrain mass from the core flow, and eventually, all of the fluid will be flushed through the boundary layers. In this way, the entire flow field will feel the effects of viscosity over a timescale of $l/(\nu\Omega)^{\frac{1}{2}}$. In fact, the form of the steady state in many geometries is dictated by this Ekman pumping.

Now consider the case where there are no Ekman layers. If the flow has closed streamlines, then Batchelor diffusion will occur between the streamlines. This is evident from (3) and (4). No matter how small we make ν, the flow will only achieve a truly steady state when diffusion between streamlines is complete. In short, a finite viscosity ensures Γ is uniform in closed-streamline regions outside the boundary layers. Equation (4) then ensures that ω_θ/r is also uniform in these regions (see Batchelor 1956). The equivalent result for buoyancy-driven flow is that T and ω_θ/r are both uniform. Clearly, viscosity plays a key role, diffusing gradients on a timescale of l^2/ν.

Now, suppose that we have an axisymmetric container, of maximum radius R and depth l. Let the lid rotate at a speed Ωr, as shown in figure 3(*a*). If the fluid has some

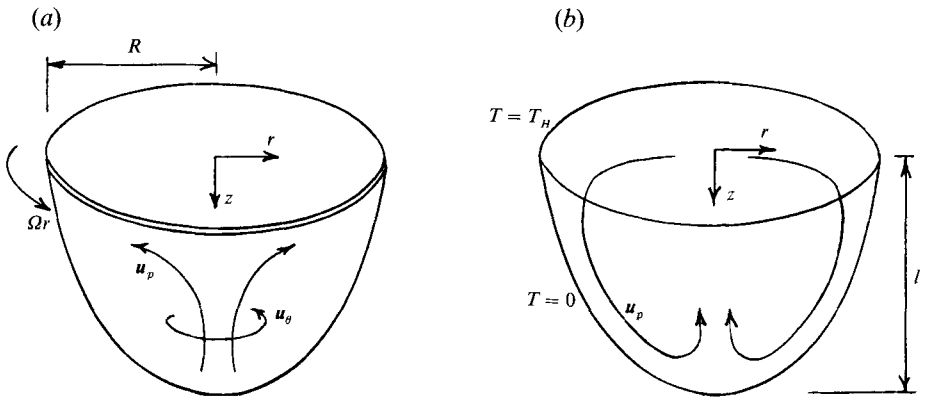

FIGURE 3. (*a*) Swirling flow in an axisymmetric container. The lid of the container rotates at angular velocity Ω. (*b*) Buoyancy flow in an axisymmetric container. The lid of the container is held at temperature T_H, and the sidewall at temperature $T = 0$.

initial velocity, it will approach steady state through a combination of damped inertial waves, operating on a timescale of Ω^{-1}, Ekman pumping, operating on a timescale of $l/(\nu\Omega)^{\frac{1}{2}}$, and Batchelor diffusion, operating on a timescale of l^2/ν.

Now intuitively, one would expect the magnitude of the recirculation in the steady state to be controlled by Ekman pumping. If this is so, then $|\boldsymbol{u}_p| \ll u_\theta$, and (9) demands that Γ is independent of z (to the appropriate order). This is reminiscent of the Taylor–Proudman theorem. Although substantially correct, the problem with this argument is that we do not know, *a priori*, whether Ekman pumping does indeed control the recirculation. There could, in principle, be other forms of steady state, such as Batchelor-like flows. Moreover, we wish to extend our results to buoyant fluids, where there are no Ekman layers. Clearly, a more formal approach is needed.

We shall examine the different possibilities using a conservation-of-energy argument similar to that of Batchelor (1956). The picture which emerges is one of stratification of Γ, with possible Batchelor-like subdomains embedded in the flow field. In addition, all of the vorticity, ω_θ, is located at the boundaries. The links between rotating and buoyant fluids suggest that an equivalent class of steady states exist where T is stratified, and this does indeed turn out to be the case. We start, however, with swirling flows. For simplicity, we shall restrict ourselves to laminar flow, although the arguments are essentially the same when the flow is turbulent.

Let us apply (3) and (4) to the final steady state. If we integrate the Navier–Stokes equation along a closed streamline, S, then we obtain

$$\oint_S \frac{\Gamma^2}{r^3}\mathrm{d}r + \nu \oint_S \nabla^2 \boldsymbol{u}_p \cdot \mathrm{d}\boldsymbol{x} = 0. \tag{15}$$

This states that, on completing a trajectory in the (r,z)-plane, the poloidal kinetic energy which is gained by a fluid particle through the action of the centripetal acceleration must be diffused or dissipated out of that particle by shear. In view of the smallness of ν, there are four ways that we can satisfy this equation. These are:

(*a*) $\boldsymbol{u}_p$ scales as ν^{-1};

(*b*) Γ is constant along the streamline, to order ν;

(*c*) the streamline passes through a boundary layer, or some other singular region, where gradients in $\boldsymbol{u}_p$ scale as $\nu^{\frac{1}{2}}$;

(*d*) Γ is independent of z, to order ν.

Now, option (*a*) can be ruled out as it requires E_p at $t \to \infty$ to be much larger than E_p at $t = 0$, despite the fact that the approach to steady state would be dissipative. Option (*b*) is the inviscid steady-state flow $\Gamma = \Gamma(\psi)$. However, we have already seen that Batchelor diffusion would reduce such streamlines to sub-domains where Γ and ω_θ/r are uniform. In general, such a structure will not satisfy all of the boundary conditions, although there may be Batchelor regions embedded in a more complex flow pattern. If we, for the moment, put aside such regions, we are left with options (*c*) and (*d*). The last of these seems particularly appealing, since it leads to a minimum-energy state for the swirl. However, we can show that, Batchelor regions apart, all the streamlines must satisfy *both* (*c*) and (*d*). We may demonstrate this as follows.

Suppose that (*d*) holds true, but (*c*) does not. Then (8) tells us that $\boldsymbol{u}_p = u_z(r)\,\hat{\boldsymbol{e}}_z$ everywhere in the core. It follows that all of the streamlines are brought into contact with the boundary, and so (*c*) must also hold true after all. Alternatively, suppose that we take option (*c*) as our starting point. Let δ be the boundary-layer thickness. Then the recirculating velocity in the von Kármán layers is of order ΩR, and continuity requires that the core recirculation is of order of $\Omega\delta$. We can now estimate the advection of vorticity, ω_θ, in the core,

$$\boldsymbol{u}\cdot\nabla(\omega_\theta/r) \sim \left(\frac{\delta}{R}\right)^2 \frac{\Omega^2}{R}.$$

Equation (9) then tells us that the axial lengthscale for Γ is

$$\frac{\partial \Gamma}{\partial z} \sim \frac{\Gamma}{R}\left(\frac{\delta}{R}\right)^2 \tag{16}$$

and we conclude that condition (*d*) is also satisfied.

Our conclusion, then, is that, with the exception of Batchelor-like sub-domains, all of the streamlines pass through the boundary layers, and in addition, the core angular momentum is independent of z. This last statement is reminiscent of the Taylor–Proudman theorem (see Greenspan 1968), the existence of which is usually established on the *a priori* assumption of a vanishingly small recirculation. Perhaps the most familiar flow field which satisfies all of the characteristics above is Ekman pumping between parallel discs rotating at different speeds.

Let us now turn to the buoyancy-driven flow shown in figure 3(*b*). The lid of the container is held at a temperature T_H, and the walls are maintained at a temperature $T = 0$. In the interests of generality, we shall make no particular assumption about the size of α. We assume only that ν is small. This case has been discussed briefly by Davidson (1992), and the arguments are similar to those used above. Given an initial state, the flow will evolve towards a steady state through a combination of internal waves, entraining boundary layers, and internal diffusion.

As before, we start our analysis by integrating the steady-state poloidal equation (5) around a closed streamline.

$$g\beta \oint_S T\,\mathrm{d}z = \nu \oint_S \nabla^2 \boldsymbol{u}\cdot\mathrm{d}\boldsymbol{r}. \tag{17}$$

The smallness of ν leaves us with four options:

(*a*) $\boldsymbol{u}$ scales as ν^{-1};

(*b*) T is constant along the streamline, to order ν;

(*c*) the streamline passes through a boundary layer, or some other singular region, where gradients scale as $\nu^{\frac{1}{2}}$;

(*d*) T is stratified and independent of r, to order ν.

As with the swirling flow, we shall dismiss (*a*) on the grounds that it implies a large kinetic energy. Provided α is small, option (*b*) will lead to Batchelor regions of uniform T and ω_θ/r, which, in general, will occupy some sub-domain of the flow field. The remainder of the streamlines must satisfy either (*c*) or (*d*). Option (*c*) implies entraining boundary layers, similar to von Kármán layers in a rotating flow, while option (*d*) represents a minimum-energy state. Not surprisingly, we find that the streamlines satisfy both (*c*) and (*d*). The arguments are very similar to those used before. To show that (*d*) implies (*c*), we use (10) to evaluate the core velocity:

$$u_{zc} = \alpha T_c''(z)/T_c'(z). \tag{18}$$

(The subscript '*c*' indicates that these are core values of T and u_z.) This expression requires that all of the streamlines pass out of the core and into the boundary layer, so that (*c*) is satisfied. Note that, in the limit of $\alpha \to 0$, the core velocity is zero, so that the recirculation does not penetrate into the stratified region.

To show that (*c*) implies (*d*), we must again revert to general scaling arguments. Let L_T be the axial lengthscale for the core temperature field. Then the boundary-layer version of (5) requires

$$u_{zb}^2/L_T \sim g\beta T_H.$$

(Here, the subscript '*b*' indicates a variable in the boundary layer.) If all the streamlines pass through this boundary layer, continuity gives

$$u_{zc} \sim (\delta/R)(g\beta T_H L_T)^{\frac{1}{2}}.$$

This allows us to estimate the transport of vorticity in the core:

$$\boldsymbol{u}\cdot\boldsymbol{\nabla}(\omega_\theta/r) \sim \frac{g\beta}{R}\left(\frac{\delta}{L_T}\right)^2 \frac{T_H}{R}.$$

With the aid of (11) we deduce

$$\frac{\partial T_c}{\partial r} \sim \frac{T_c}{R}\left(\frac{\delta}{L_T}\right)^2$$

from which we conclude that condition (*d*) is indeed satisfied.

For buoyancy-driven flow, then, all of the streamlines pass through the boundary layer and, in addition, the core is thermally stratified. This is precisely what is seen in the high-Prandtl-number experiments of Elder (1965), as well as in the low-Prandtl-number experiments of Vives & Perry (1988).

The idea of a thermally stratified core seems to have come first from Gill (1966) who analysed two-dimensional flow in a slot. In his case, the Prandtl number was of order one, so that the two-dimensional equivalent of (18) implies that the core flow is horizontal. In his analysis, the boundary layers both entrain and detrain in such a way that one feeds the other via the core. This is analogous to Ekman pumping between parallel discs rotating at different speeds. Unlike the Ekman problem, however, Gill's analysis is only approximate, the boundary layers being treated in a somewhat simplified manner.

There is a direct equivalence, then, between thermal stratification and the Taylor–Proudman theorem. The general shape of the isotherms and Γ-lines in buoyancy-driven and centrifugal flows are shown in figure 4. Having established the generic structure of these steady states, we now look at an approximate means of predicting the magnitude of the flow fields. We start, in §5, with swirling flow. Subsequently, in §6, we tackle buoyancy-driven flow. In each case, we resort to a momentum-integral technique for handling the boundary layers. Such an approach inevitably carries with it a potential loss of accuracy, so we shall compare our predictions with numerical experiments.

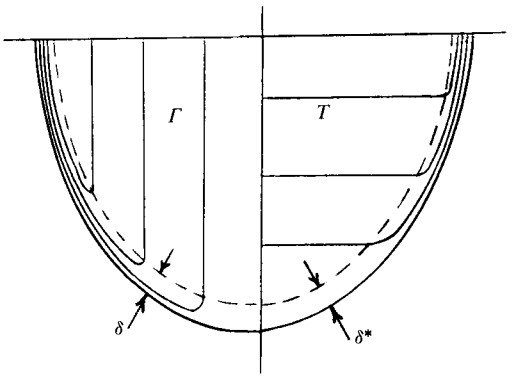

FIGURE 4. A comparison of the isotherms for thermally induced flow with the constant-angular-momentum lines of a swirling flow.

5. Momentum integral analysis of swirling flow

In this section we will take the boundary layers to be turbulent, largely because most flows encountered in practice are indeed turbulent. We shall use the coordinate system shown in figure 5, in addition to r and z, we introduce the curvilinear coordinates s and n to define a point relative to the sidewall. The normal and tangential vectors are $\boldsymbol{n}$ and $\boldsymbol{t}$, and ϕ defines the angle of the surface to the horizontal. The surface coordinates are denoted (r_s, z_s).

If we integrate (3) through the boundary layer on the sidewall, from $n = 0$ to δ, we obtain

$$\frac{\mathrm{d}}{\mathrm{d}s}\left\{r_s \int_0^\delta [\Gamma_c - \Gamma] u_s \,\mathrm{d}n\right\} - \frac{\dot{q}}{2\pi}\frac{\mathrm{d}\Gamma_c}{\mathrm{d}s} = \frac{r_s^2}{\rho}\tau_\theta. \tag{19}$$

Here $\Gamma_c(r)$ is the core angular momentum, u_s is the tangential velocity in the boundary layer, τ_θ is the wall shear stress, and $\dot{q}$ is the mass flux in the boundary layer,

$$\frac{\dot{q}}{2\pi r_s} = \int_0^\delta u_s \,\mathrm{d}n. \tag{20}$$

A slightly different formulation is required for the boundary layer under the top surface. Here the lid of the container rotates faster than the fluid, at a speed of Ωr. Consequently, the boundary-layer momentum-integral equation for the lid is the same as (19), but with the sign of the shear stress reversed:

$$\frac{\mathrm{d}}{\mathrm{d}r}\left\{r \int_0^\delta [\Gamma - \Gamma_c] u_r \,\mathrm{d}z\right\} + \frac{\dot{q}}{2\pi}\frac{\mathrm{d}\Gamma_c}{\mathrm{d}r} = \frac{r^2}{\rho}\tau'_\theta. \tag{21}$$

Here τ'_θ is the surface shear stress on the lid. Following Greenspan (1968), we estimate the stresses τ_θ and τ'_θ using the well-known seventh-power-law fit to the law of the wall. This fixes the wall shear as

$$\tau = 0.0225\rho u^2(\nu/u\delta)^{\frac{1}{4}},$$

where u is the slip velocity between the core and the wall. In the present context, this gives

$$r_s^2\tau_\theta/\rho = \kappa_1 \Gamma_c^2$$

and

$$r^2\tau'_\theta/\rho = \kappa_2(\Omega r^2 - \Gamma_c)^2,$$

where κ_1 and κ_2 are the coefficients

$$\kappa_1 = 0.0225[\nu r_s/\Gamma_c\delta]^{\frac{1}{4}}, \qquad \kappa_2 = 0.0225[\nu r/(\Omega r^2 - \Gamma_c)\delta]^{\frac{1}{4}}.$$

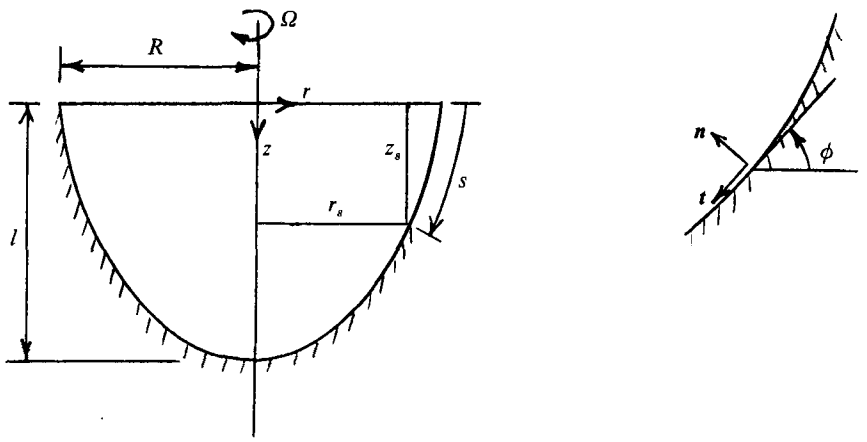

FIGURE 5. Coordinate system.

Now the coefficients, κ_1 and κ_2, will typically vary as $r^{-\frac{1}{4}}$, depending on the rate of growth of δ. Since this dependence on r is much less than the dependence of the parameters they multiply (that is, $\Gamma^2 \sim r^4$), we will make the judicious approximation of treating κ_1 and κ_2 as constants.

Next, we consider the recirculation in the core. Since Γ_c is materially advected, it follows that the core velocity is

$$\boldsymbol{u}_c = u_z(r)\,\hat{\boldsymbol{e}}_z.$$

As a consequence, the mass flux in the top boundary layer, at any particular radius, is equal to the mass flux in the bottom boundary layer, at the same radius. Thus, we may write $\dot{q} = \dot{q}(r)$.

Finally, it is convenient to introduce the shape coefficients χ_s and χ_t, defined by

$$\int_0^\delta (\Gamma_c - \Gamma)\,u_s\,\mathrm{d}n = \chi_s \Gamma_c \frac{\dot{q}}{2\pi r_s}, \qquad \int_0^\delta (\Gamma - \Gamma_c)\,u_r\,\mathrm{d}z = \chi_t(\Omega r^2 - \Gamma_c)\frac{\dot{q}}{2\pi r}.$$

As is conventional with momentum-integral analysis, we treat χ_s and χ_t as independent of s. Their magnitude may be estimated by assuming that the profiles for Γ and u_s follow the seventh-power-law. For example, in the sidewall boundary layer, we follow von Kármán (1921) and write,

$$\frac{u}{\hat{u}} = \left(\frac{n}{\delta}\right)^{\frac{1}{7}}\left[1 - \left(\frac{n}{\delta}\right)\right], \quad \frac{\Gamma}{\Gamma_c} = \left(\frac{n}{\delta}\right)^{\frac{1}{7}},$$

which gives $\chi_s = \frac{1}{6}$. An equivalent expression for the top boundary layer also gives $\chi_t = \frac{1}{6}$. Equations (19) and (21) now reduce to

$$\frac{1}{6}\frac{\mathrm{d}}{\mathrm{d}r}\left\{\Gamma_c \frac{\dot{q}}{2\pi}\right\} - \frac{\dot{q}}{2\pi}\frac{\mathrm{d}\Gamma_c}{\mathrm{d}r} = \kappa_1 \Gamma_c^2 \frac{\mathrm{d}s}{\mathrm{d}r_s}, \tag{22}$$

$$\frac{1}{6}\frac{\mathrm{d}}{\mathrm{d}r}\left\{(\Gamma_W - \Gamma_c)\frac{\dot{q}}{2\pi}\right\} + \frac{\dot{q}}{2\pi}\frac{\mathrm{d}\Gamma_c}{\mathrm{d}r} = \kappa_2(\Gamma_W - \Gamma_c)^2, \tag{23}$$

where $\Gamma_W = \Omega r^2$. Provided we can evaluate δ, and so find κ_1 and κ_2, we have two equations in two unknowns, $\Gamma_c(r)$ and $\dot{q}(r)$. The boundary-layer thickness, δ, is determined by the poloidal component of the momentum-integral equation.

Consider, by way of an example, the case of a cone, with a half-angle of $\frac{1}{2}\pi - \phi$. Then (22) and (23) are satisfied if we take

$$\Gamma_c = \Omega_c r^2, \quad \dot{q}/2\pi r = cr^2,$$

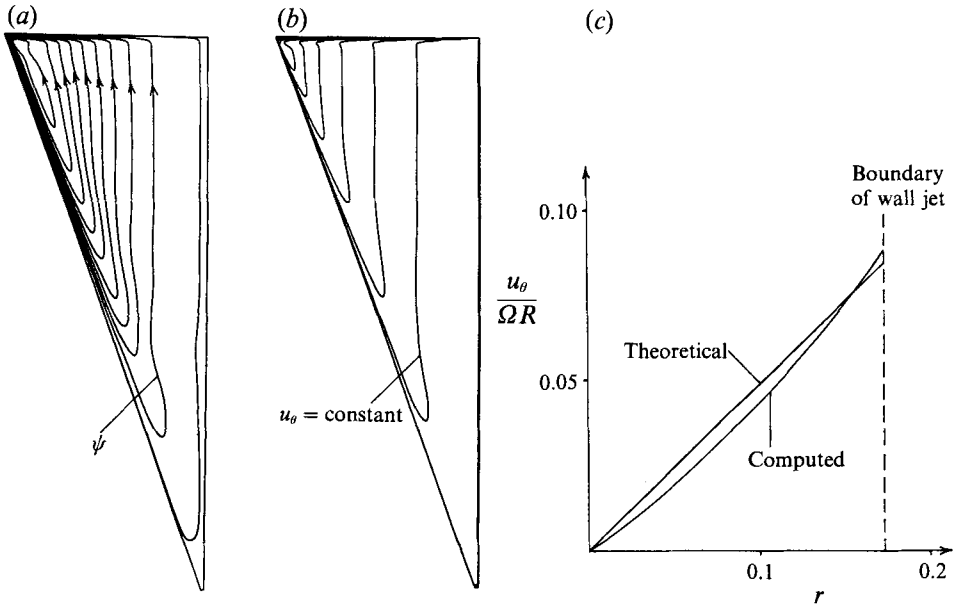

FIGURE 6. Finite difference calculation of forced swirl in a cone of half-angle 20°. (*a*) Streamfunction, (*b*) contours of constant u_θ, (*c*) variation of u_θ with r for a slice through the cone ($z = 0.243$ m).

and these substitutions give us

$$7\frac{\kappa_2}{\kappa_1}\cos\phi\left(\frac{\Omega}{\Omega_c}-1\right)^2-5\left(\frac{\Omega}{\Omega_c}-1\right)-12=0, \quad c=\tfrac{6}{7}\kappa_1\Omega_c/\cos\phi.$$

Noting that,

$$\frac{\kappa_2}{\kappa_1}\approx\left(\frac{\Omega_c}{\Omega-\Omega_c}\right)^{\frac{1}{4}}$$

the first of these relationships gives an explicit expression for the core angular velocity, Ω_c, in the cone:

$$7\cos\phi\left(\frac{\Omega}{\Omega_c}-1\right)^{\frac{7}{4}}-5\left(\frac{\Omega}{\Omega_c}-1\right)-12=0. \tag{24}$$

For example, consider a cone with a half-angle of 20°. Then (24) gives a core angular momentum distribution of

$$\Gamma_c(r)=0.177\Omega r^2.$$

We have computed this flow using a finite difference code. The fluid is water, the height of the cone was taken to be 1 m, and the rotation rate of the lid is 10 rad/s. The k–ϵ turbulence model was used to estimate the shear stress, with no correction made for the influence of swirl on the Reynolds stresses. The results are shown in figure 6. Figure 6(*a*), shows ψ, and it is clear that all of the streamlines do indeed pass through the boundary layers. Figure 6(*b*) shows the contours of constant u_θ. Note that, as predicted, u_θ is virtually independent of z. Finally, figure 6(*c*) shows the radial variation in u_θ for a slice through the cone at $z = 0.243$ m. The theoretical prediction of $u_\theta = (1.77\text{ rad/s})r$ is also shown. In view of the rather substantial approximations that are associated with the momentum-integral method, this comparison seems not unfavourable.

Let us now consider the analogous buoyancy-driven flow.

6. Momentum-integral analysis of buoyancy-driven flows

If we refer back to figure 4, showing a thermally stratified core, it is clear that there will be thermal boundary layers on the sidewalls. A closely related problem has been solved by Prandtl (1952). He considered the case of a V-shaped valley, where the air temperature in the valley is thermally stratified, but where the temperature of the slopes is everywhere lower than that of the ambient air. Away from the slopes, there is no motion, as the stratified air is supported by a hydrostatic pressure distribution. Near the edges, however, the air temperature adjusts to that of the slopes, and a thermal boundary layer develops. Prandtl showed that, within the relatively thin boundary layer, jets of high-speed cold air flow down the slopes. These jets then collide at the base of the valley, forming a 'river' of air flowing along the valley floor. (In our axisymmetric case, of course, this flow is forced to recirculate back through the core.) We shall see that these Prandtl boundary layers adopt the role previously played by Ekman layers.

As before, we shall use the coordinate system shown in figure 5. This time, we shall take $\phi = \frac{1}{2}\pi$ at $s = 0$, so the sidewall is initially vertical. Also, we shall take the upper surface temperature to be T_H, and the sidewall temperature to be zero.

Let the thermal boundary-layer thickness be δ^*. So far, we have not specified the size of α. We shall take α to be small, so that $\delta^* \ll R$, but not so small that equation (18) excludes any flow in the stratified part of the core. Formally, we shall look at the limit

$$\nu \ll \alpha \ll uR.$$

This hierarchy is typical of the flow of liquid metals, where the Reynolds number is usually large, but the Prandtl number is small. One consequence of this restriction is that the thermal boundary layer is much thicker than the momentum boundary layer. Consequently, the thickness of the jet at the sidewall is dictated by δ^* rather than δ.

As before, we introduce the boundary-layer mass flux $\dot{q}$, which, from (18), can be expressed in terms of the core temperature, $T_c(z)$:

$$\frac{\dot{q}}{2\pi r_s} = \int_0^{\delta^*} u_s \, \mathrm{d}n = -\frac{\alpha r_s}{2} \frac{T_c''(z)}{T_c'(z)}. \tag{25}$$

Next, it is useful to define four coefficients, χ_1 to χ_4, which depend on the shape of the velocity and temperature profiles in the thermal boundary layer:

$$\left(\frac{\partial T}{\partial n}\right)_0 = \chi_1 \frac{T_c}{\delta^*}, \quad \int_0^{\delta^*} u_s^2 \, \mathrm{d}n = \frac{\chi_2}{\delta^*}\left[\frac{\dot{q}}{2\pi r_s}\right]^2,$$

$$\int_0^{\delta^*} (T_c - T) \, \mathrm{d}n = \chi_3 T_c \delta^*, \quad \int_0^{\delta^*} u_s (T_c - T) \, \mathrm{d}n = \chi_4 T_c \left[\frac{\dot{q}}{2\pi r_s}\right].$$

In accordance with the conventional momentum-integral approach, we treat these coefficients as independent of s. We can now write down the momentum-integral equations for the sidewall, obtained from integrating (5) and (6) through the thermal boundary layer. These are given in Davidson (1992) as

$$\chi_2 \frac{\mathrm{d}}{\mathrm{d}s}\left\{\frac{1}{r_s \delta^*}\left(\frac{\dot{q}}{2\pi}\right)^2\right\} = g\beta r_s \sin\phi(\chi_3 T_c \delta^*) - \frac{r_s \tau_W}{\rho},$$

$$\chi_4 \frac{\mathrm{d}}{\mathrm{d}s}\left\{T_c\left(\frac{\dot{q}}{2\pi}\right)\right\} - \frac{\dot{q}}{2\pi}\frac{\mathrm{d}T_c}{\mathrm{d}s} = \alpha r_s \left\{\chi_1 \frac{T_c}{\delta^*} - T_c'(z)\frac{\mathrm{d}r_s}{\mathrm{d}s}\right\}.$$

Now, in the early stages of development of the wall jet, the momentum boundary layer will be much thinner than the thermal boundary layer. Consequently, we may neglect τ_W in the equations above, provided we restrict attention to the initial part of the wall jet. (Formally, we are then integrating the equations from $n = \delta$ to δ^*, rather than from $n = 0$ to δ^*.) If we now substitute for $\dot{q}$, using (25), we find

$$\frac{\mathrm{d}}{\mathrm{d}s}\left\{\frac{r_s^3}{\delta^*}\left(\frac{T_c''}{T_c'}\right)^2\right\} = \frac{\chi_3}{\chi_2}\frac{4g\beta}{\alpha^2} r_s \sin\phi T_c \delta^*, \tag{26}$$

$$\frac{\mathrm{d}}{\mathrm{d}s}\left\{\chi_4 r_s^2 T_c\left(\frac{T_c''}{T_c'}\right) - r_s^2 T_c'\right\} = -2\chi_1 \frac{r_s}{\delta^*} T_c. \tag{27}$$

In order to evaluate the constants χ_1 to χ_4, we must adopt some 'shape function' for the velocity and temperature profiles. Since it is not obvious what these shapes should be, we shall evaluate χ_i for the boundary layer near $s = 0$. At this point, the problem looks locally like that of a cold, vertical plate immersed in a fluid of uniform temperature, T_H. (We ignore the vertical gradient in T_c.) The governing equations are then

$$\left\{u_s\frac{\partial}{\partial s} + u_n\frac{\partial}{\partial n}\right\}\frac{\partial u_s}{\partial n} = -g\beta\frac{\partial T}{\partial n}, \quad \left\{u_s\frac{\partial}{\partial s} + u_n\frac{\partial}{\partial n}\right\} T = \alpha\frac{\partial^2 T}{\partial n^2}.$$

As with Pohlhausen's classic solution for a viscous wall jet (see Turner 1973), we can extract an exact solution by scaling δ^* and u_s as $\delta^* \sim s^{\frac{1}{4}}$ and $u_s \sim s^{\frac{1}{2}}$. In particular, we write

$$n = \eta\left\{\frac{4\alpha^2 s}{g\beta T_H}\right\}^{\frac{1}{4}}, \quad u_s = (4g\beta T_H)^{\frac{1}{2}} s^{\frac{1}{2}} h'(\eta), \quad T = T_H f(\eta).$$

Our partial differential equations then reduce to,

$$2h'(\eta)^2 - 3hh''(\eta) = 1 - f, \quad f''(\eta) + 3hf'(\eta) = 0. \tag{28a, b}$$

These are readily integrated subject to the boundary conditions: $f(0) = 0$, $f(\infty) = 1$, $h(0) = 0$, and $h'(\infty) = 0$. We see immediately from these boundary conditions that the velocity at the wall is

$$u_s(0) = (2g\beta T_H)^{\frac{1}{2}} s^{\frac{1}{2}}.$$

The numerical solution of these equations is reported in Schlichting (1979). For our purposes, a good approximation to this solution is given by

$$h'(\eta) = \frac{1}{\sqrt{2}}\exp(-1.456\eta),$$

where f is then found from (28*a*). It follows that

$$\chi_1 = 2.13, \quad \chi_2 = 2.13, \quad \chi_3 = 0.294, \quad \chi_4 = \tfrac{7}{12}.$$

The next step is to recast (26) and (27) in dimensionless form. Let us introduce a modified Grashof number, based on α rather than ν:

$$Gr^* = g\beta R^3 T_H/\alpha^2. \tag{29}$$

Typically, in a liquid-metal flow, this is of the order of 10^5–10^7. Inspection of (26) and (27) shows that the characteristic axial lengthscale in the stratified region is

$$L_T = (Gr^*)^{-\frac{1}{7}} R.$$

It follows that the boundary-layer velocity, core velocity, and boundary-layer thickness each scale as

$$u_b \sim (\alpha/R)(Gr^*)^{\frac{3}{7}}, \quad u_c \sim (\alpha/R)(Gr^*)^{\frac{1}{7}}, \quad \delta^* \sim R(Gr^*)^{-\frac{2}{7}}.$$

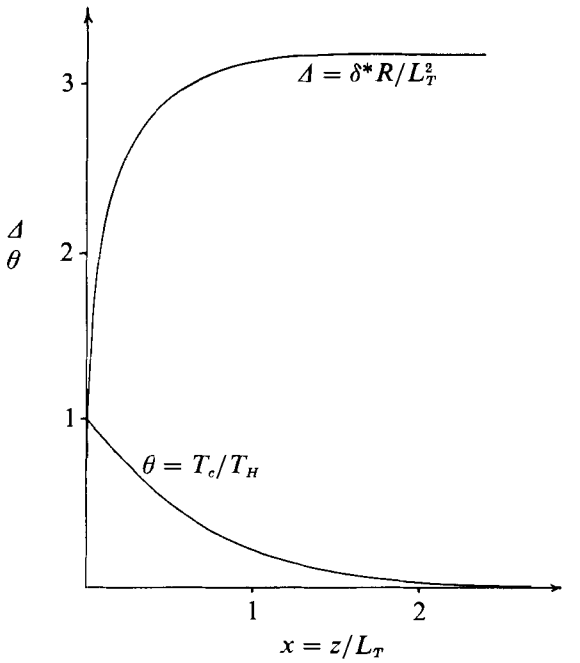

FIGURE 7. Momentum-integral predictions of temperature, θ, and boundary-layer thickness, Δ, for buoyancy-driven flow.

Consequently, it is useful to introduce the scaled variables,

$$x = z/L_T, \quad \theta(x) = T_c(z)/T_H, \quad \Delta(x) = \delta^* R/L_T^2.$$

Additionally, since $L_T \ll R$, we can put $\phi = \frac{1}{2}\pi$ and $r_s = R$ in our boundary-layer equations. In other words, the stratified region is confined to the top of the flow field, the rest of the core being a Batchelor region at $T = 0$, where our equations are no longer valid. The simplified boundary-layer equations are then

$$\frac{\mathrm{d}}{\mathrm{d}x}\left\{\frac{1}{\Delta}\left(\frac{\theta''}{\theta'}\right)^2\right\} = 0.553\theta\Delta, \tag{30}$$

$$\frac{\mathrm{d}}{\mathrm{d}x}\left\{\theta' - \frac{7}{12}\frac{\theta\theta''}{\theta'}\right\} = 4.25\frac{\theta}{\Delta}, \tag{31}$$

which may be integrated subject to the boundary conditions: $\theta(0) = 1, \theta(\infty) = 0$, $\Delta(0) = 0$. The initial solution, which satisfies $\theta(0) = 1$ and $\Delta(0) = 0$, is

$$\theta(x) = 1 + \theta'(0)\{x - 0.528x^{\frac{11}{4}} + \ldots\}, \quad \Delta(x) = 3.82x^{\frac{1}{4}} + \ldots.$$

The unknown constant, $\theta'(0)$, is determined by the boundary condition at $x = \infty$. The solutions for Δ and θ over the whole range are shown in figure 7. The depth of the stratified region, taken to be the point where θ falls to 0.02, is predicted to be

$$L_s = 2.29R(Gr^*)^{-\frac{1}{7}},$$

and the peak boundary-layer mass flux is predicted to be

$$\dot{q} = 1.78\pi R\alpha(Gr^*)^{\frac{1}{7}}.$$

In order to test the validity of these predictions, we have computed the buoyancy-driven flow in a cylinder. We used the same finite-difference code discussed in §5. The

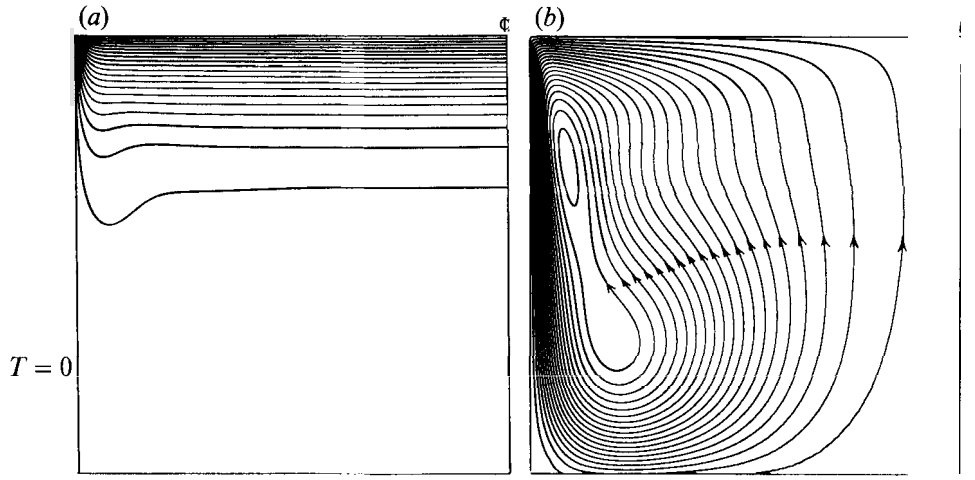

FIGURE 8. Buoyancy-driven flow in a cylinder with the top surface at $T_H = 100$ °C: (*a*) isotherms, (*b*) streamfunction.

liquid properties were taken as, $\rho = 2380$ kg/m^3, $\beta = \mathbf{10^{-4}\ K^{-1}}$, $\alpha = \mathbf{4.67 \times 10^{-5}}$ m/s, and $\nu = 5.46 \times 10^{-7}$ m^2/s. The cylinder was given a radius and height of 0.3 m. Two cases were examined: $T_H = 50$ °C and 100 °C. The isotherms and streamfunction for the case where $T_H = 100$ °C are shown in figure 8. As expected, we have a quiescent, thermally stratified fluid in the upper part of the cylinder, a Batchelor region below, and pronounced wall jets on the sidewalls. The depth of the stratified region is computed to be 0.115 m for the case where $T_H = 50$ °C, and 0.104 m for $T_H = 100$ °C. The ratio of these two depths, which is indicative of the scaling of L_s on T_H, is 0.904. Our approximate theory predicts L_s to be 0.103 m and 0.093 m respectively, corresponding to a ratio of depths of 0.906. The two predictions of L_s seem to be reasonably in accord, with a maximum discrepancy of 11%. The peak boundary-layer mass flux for the two cases are computed to be 5.69×10^{-4} m^3/s and $6.56 \times \mathbf{10^{-4}}$ m^3/s (ratio = 1.15), whereas our theoretical model predicts 5.22×10^{-4} m^3/s and $5.77 \times \mathbf{10^{-4}}$ m^3/s (ratio = 1.11). Our analysis appears to underestimate the maximum mass flux by $\sim$ 12%. This may be due to our assumed shape function for the wall jet. Nevertheless, there is a reasonably good match between the theoretical model and the computations.

7. Steady-state solutions of the inviscid equations of motion

It is clear from the preceding sections that a finite viscosity, no matter how small, has profound implications for the structure of closed-streamline steady-state flows. Nevertheless, for completeness, we conclude this paper by examining steady-state solutions of the inviscid equations. It is likely that these flows, for the most part, are unstable. Moreover, it is by no means clear just how such a flow could be initiated. However, any stable solution which does exist could, in principle, persist in a real fluid for a short period, before (Batchelor) diffusion alters its structure. Such flows, if they exist, would be of interest in their own right. We start with swirling flows.

As noted in §2, equations (8) and (9) admit two classes of steady solution. The first is the degenerate case $\Gamma = \Gamma(r), \psi = 0$. The second is

$$\Gamma = \Gamma(\psi), \tag{32}$$

$$\omega_\theta / r = \Gamma\Gamma'(\psi)/r^2 - H'(\psi). \tag{33}$$

It turns out that H is Bernoulli's constant. Solutions of (32) and (33) are readily found when all of the streamlines originate at $z = -\infty$. In such a case, Γ and H can be specified at some upstream location.

When the streamlines are closed, however, the situation is far less simple. Only a few solutions are known. Moffatt (1969) has found one solution of the form $\Gamma = a\psi$. This is a generalization of Hill's spherical vortex. The vorticity and swirl are confined to a sphere which itself sits in a transverse, irrotational flow. Interestingly, the external flow over the sphere may be set to zero by the appropriate choice of a. In a later paper, Moffatt (1988) used the device of magnetic relaxation to establish the existence of a more general set of solutions of (32) and (33), also consisting of a localized blob of vorticity and swirl. Finally, Davidson (1989) noted a solution for flow enclosed in a cylinder. Again, the solution has the form, $\Gamma = a\psi$, and is a Beltrami flow with $\omega = a\boldsymbol{u}$.

Unfortunately, we do not know whether any of the solutions described above are stable. (By stable, we mean stable with respect to axisymmetric disturbances.) Certainly, they all contain regions where $\Gamma'(r) < 0$, suggesting the potential for a Rayleigh instability. The question of stability is perhaps best addressed through the method developed by Vallis *et al.* (1988), which relies on Arnol'd's stability theorems. (See Drazin & Reid 1981 for an account of Arnol'd's theorems.)

To establish stability of an inviscid steady state, Arnol'd advected the vorticity field using a virtual displacement, $\boldsymbol{\eta}(\boldsymbol{x})$, with $\nabla \cdot \boldsymbol{\eta} = 0$, and $\boldsymbol{\eta}\, \mathrm{d}\boldsymbol{s} = 0$ at the boundary. He then showed that, since $\boldsymbol{u}$ is a steady state, the kinetic energy of the flow has a stationary value, $\delta^1 E = 0$. Moreover, the flow is stable only if this stationary value is either a maximum or a minimum. That is, stability requires $\delta^2 E$ to be of definite sign for all possible displacement fields $\boldsymbol{\eta}$. Building on the work of Moffatt (1986), Vallis *et al.* adapted Arnol'd's analysis in the following way. They introduced a form of 'modified dynamics', described by

$$\partial \boldsymbol{\omega}/\partial t = \nabla \times (\hat{\boldsymbol{u}} \times \boldsymbol{\omega}), \tag{34}$$

$$\hat{\boldsymbol{u}} = \boldsymbol{u} + \lambda\, \partial \boldsymbol{u}/\partial t. \tag{35}$$

Here we may think of $\hat{\boldsymbol{u}}$ as a continuously evolving form of Arnol'd's displacement field which is functionally related to the instantaneous velocity, $\boldsymbol{u}$. These equations have three important properties. Firstly, the vorticity is smoothly advected by $\hat{\boldsymbol{u}}$. It follows that all the normal invariants of the vorticity field, such as circulation and helicity, are conserved. Secondly, the energy of the flow field monotonically increases or decreases, depending on the sign of λ. In fact, if we take the product of $\hat{\boldsymbol{u}}$ with the 'uncurled' form of (34), we may show that

$$\dot{E}(t) = \frac{\partial}{\partial t} \int_V \tfrac{1}{2}\boldsymbol{u}^2\, \mathrm{d}V = -\lambda \int_V \left(\frac{\partial \boldsymbol{u}}{\partial t}\right)^2 \mathrm{d}V.$$

Thirdly, the change in energy ceases only when the flow reaches a steady state, and in this case (34) and (35) revert to the conventional Euler equations.

Given an initial condition, the scheme will produce either $E = 0$, $E \to \infty$ or $E \to E_0$, where E_0 is finite. In the latter case, E_0 will be either a local maximum or minimum in energy, depending on the sign of λ. If the modified dynamics do settle on such a state, then Arnol'd's theorem tells us this is a stable steady solution of the Euler equations.

Vallis *et al.* used this technique to good effect in two-dimensional flows, where a non-trivial (finite E) solution is guaranteed when $\lambda < 0$. This is because, in two dimensions, the kinetic energy is bounded from above when the integral of the vorticity is conserved.

This scheme could be applied to swirling flow as it stands. However, it may be simplified somewhat if we write

$$\hat{\boldsymbol{u}} = \boldsymbol{u} + \lambda\, \partial \boldsymbol{u}_p/\partial t \tag{36}$$

instead of (35). Equation (34) then gives,

$$\hat{\mathrm{D}}\Gamma/\mathrm{D}t = 0, \tag{37}$$

$$\frac{\hat{\mathrm{D}}}{\mathrm{D}t}\left(\frac{\omega_\theta}{r}\right) = \nabla\cdot\left[\frac{\Gamma^2}{r^4}\hat{\boldsymbol{e}}_z\right] \tag{38}$$

and

$$\dot{E}(t) = -\lambda \int_V (\partial \boldsymbol{u}_p/\partial t)^2\, \mathrm{d}V. \tag{39}$$

Here $\hat{\mathrm{D}}/\mathrm{D}t$ is the convective derivative based on the advecting velocity $\hat{\boldsymbol{u}}$. A comparison with (8) and (9) shows that the modified transport equations above have precisely the same form as the originals, but with a convective derivative based on $\hat{\boldsymbol{u}}$, rather than $\boldsymbol{u}$. As before, angular momentum is materially conserved, so that $\int \Gamma\, \mathrm{d}V$ is constant. (This is not surprising, as Γ is the streamfunction for ω_p.) It follows immediately that we may apply (14) to our modified flow, and so impose a lower bound on E. Consequently, provided we take $\lambda > 0$, any initial flow is guaranteed to evolve to a stable, steady solution of the Euler equations. (In practice, of course, singularities such as vortex sheets may well develop.)

Curiously, these steady states correspond to a local minimum in energy, whereas the two-dimensional flows computed by Vallis *et al.* correspond to local maxima. In fact, in two dimensions, E is bounded from above, by conservation of global vorticity, but not necessarily from below. (As Vallis *et al.* 1989 shows, Kelvin's 'vortex sponge' allows E to tend to zero, while preserving global vorticity.) Conversely, in axisymmetric, swirling flow, E is bounded from below, but not from above. (We can produce an infinite kinetic energy by pulling a fluid element with finite Γ to the axis.)

We can gain some small insight into the mechanics of the modified dynamics by considering a very simple case. Suppose that, at $t = 0$, we have a velocity field given by

$$\Gamma = \Omega r^2 + \delta\Gamma, \quad \boldsymbol{u}_p = 0.$$

Then, at least initially, we may linearize (37) and (38) to give

$$\frac{\partial^2}{\partial t^2}(\nabla_*^2 \psi) + (2\Omega)^2 \frac{\partial^2}{\partial z^2}\left(\psi + \lambda \frac{\partial \psi}{\partial t}\right). \tag{40}$$

Comparing (40) with (12) shows that we have a slightly modified inertial wave. If we restrict the flow to a cylinder of radius R, then this equation supports progressive waves of the form

$$\psi = \psi_0 r J_1(\delta_n r/R) \exp(st - \mathrm{i}kx),$$

where δ_n is the nth zero of J_1. The dispersion equation is readily shown to be

$$s = -\tfrac{1}{2}\lambda\omega_0^2 \pm j\{\omega_0^2 - (\tfrac{1}{2}\lambda\omega_0^2)^2\}^{\frac{1}{2}}.$$

Clearly, the modified dynamics produces damped waves (for $\lambda > 0$), so that energy is continually extracted from the flow field until $\delta\Gamma = 0$. For a large enough value of λ, the waves are critically damped.

Now, we already know from the general form of (34) that helicity must be conserved by the modified dynamics. That is,

$$\frac{\hat{\mathrm{D}}}{\mathrm{D}t}\int_{V_\Gamma} \boldsymbol{u}\cdot\boldsymbol{\omega}\, \mathrm{d}V = 0,$$

where V_Γ is any material volume bounded by the toroidal surface $\Gamma =$ constant. It is natural to ask if there are other integral invariants of the flow when the Γ-lines are closed. That this is indeed the case follows directly from (37) and (38). These can be rearranged to give

$$\frac{\hat{\mathrm{D}}}{\mathrm{D}t}\left\{\frac{\omega_\theta}{r}g(\Gamma)+f(\Gamma)\right\} = \nabla\cdot\left\{\frac{2}{r^4}\int_0^\Gamma g(\Gamma)\,\Gamma\,\mathrm{d}\Gamma\hat{\boldsymbol{e}}_z\right\},$$

where g and f are arbitrary functions of Γ. Following the procedure outlined in §2, we find

$$\frac{\hat{\mathrm{D}}}{\mathrm{D}t}\int_{V_\Gamma}\left[\frac{\omega_\theta}{r}g(\Gamma)+f(\Gamma)\right]\mathrm{d}V = 0. \tag{41}$$

Consequently, we can ensure that all of the integral characteristics of the form

$$I = \int_{V_\Gamma}\left[\frac{\omega_\theta}{r}g(\Gamma)+f(\Gamma)\right]\mathrm{d}V \tag{42}$$

are carried over from the initial velocity field to the final steady state. This includes the signature function, $V_\Gamma(\Gamma)$. We might be tempted to speculate, therefore, that a variety of stable steady solutions of the inviscid equations of motion do exist, and that (41) ensures that they have a non-trivial topology. However, we shall see, through the analogy with buoyancy, that this is not the case. In particular, (41) is not sufficient to avoid the degenerate case $\Gamma = \Gamma(r)$.

Let us construct a similar body of theory to describe buoyancy-driven flows. To investigate the stability of such flows, we introduce a scheme where $\boldsymbol{u}$ is replaced by $\hat{\boldsymbol{u}}$ in (10) and (11). That is,

$$\hat{\mathrm{D}}T/\mathrm{D}t = 0, \tag{43}$$

$$\frac{\hat{\mathrm{D}}}{\mathrm{D}t}\left(\frac{\omega_\theta}{r}\right) = \frac{g\beta}{r}\frac{\partial T}{\partial r}, \tag{44}$$

$$\hat{\boldsymbol{u}} = \boldsymbol{u}+\lambda\,\partial\boldsymbol{u}/\partial t. \tag{45}$$

If the fluid is held in the fixed domain V, then this system of equations ensures that the total energy monotonically decreases, while preserving the expected vorticity integrals. Specifically,

$$\frac{\partial}{\partial t}\int_V (\tfrac{1}{2}\boldsymbol{u}^2+g\beta Tz)\,\mathrm{d}V = -\lambda\int_V\left(\frac{\partial\boldsymbol{u}}{\partial t}\right)^2\mathrm{d}V \tag{46}$$

and

$$\frac{\hat{\mathrm{D}}}{\mathrm{D}t}\int_{V_T}\left\{\frac{\omega_\theta}{r}g(T)+f(T)\right\}\mathrm{d}V = 0, \tag{47}$$

where V_T is a material volume bounded by an isothermal surface.

We shall now show that (47) is not a sufficient constraint to avoid degenerate (stratified) solutions of the buoyancy equations and that, by implication, (41) cannot ensure non-trivial solutions of the swirl equations. To this end, consider a variant of Moffatt's (1985) 'squeeze-film' problem. Suppose that we start with a blob of hot fluid, surrounded by cold fluid, and all contained in a cylinder of radius R. Let us choose λ to be small, so that, initially, the flow behaves in a conventional way. The blob will rise, hit the roof of the box, and spread horizontally. The cold fluid which was initially adjacent to the surface will, in principle, remain there forever, blocking the hot fluid from reaching the top of the box. However, the cold fluid will be squeezed out as

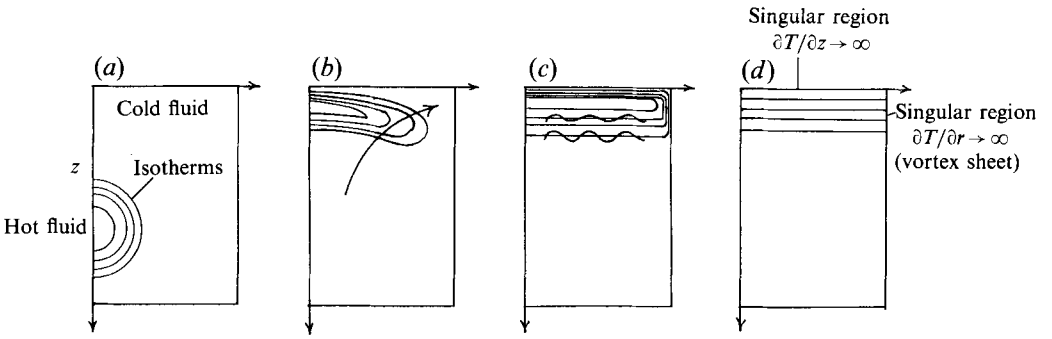

FIGURE 9. Moffatt's 'squeeze-film' process adapted to modified dynamics. (*a*) Initial state; (*b*) hot fluid rises; (*c*) fluid is almost stratified and kinetic energy is lost via damped waves; (*d*) final state is purely stratified with a vortex sheet at $r = R$.

$t \to \infty$, as shown in figure 9. Once the flow approaches stratification, the excess kinetic energy which has been gained by the fluid due to the fall in potential energy can be eliminated by damped gravity waves, analogous to (40). What we end up with then is a perfectly stratified fluid, with singular regions adjacent to the boundary. In particular, we might note that a sheet of vorticity, ω_θ, forms on the surface $r = R$.

In principle, the same process can occur if we have some initial vorticity, ω_θ, in the flow. Equation (47) is satisfied by pushing all of the initial vorticity into the vortex sheet at $r = R$. This configuration not only minimizes the potential energy, but also the total kinetic energy which is inevitably associated with a finite integral of ω_θ. (For a given net vorticity we can minimize the kinetic energy by pushing the vorticity to the boundaries.)

It seems physically plausible, therefore, that the modified dynamics of Vallis *et al.* results (at least for small λ) in the degenerate, stratified state $T = T(z)$. We can construct a similar argument to suggest that, if λ is small, minimizing the energy of a swirling flow leads to $\Gamma = \Gamma(r)$, with all of the vorticity, ω_θ, deposited at the outer radial boundary.

Now the arguments above show that the degenerate states $T(z)$ and $\Gamma(r)$ are one possible result of the modified dynamics. However, they do not prove that the modified dynamics always lead to stratification, although this does seem plausible. To help resolve this issue, we have attempted some numerical experiments. Unfortunately, in each case, the growth of singularities in the flow induced a numerical instability. (Whether or not the modified dynamics invariably generate singularities is an important issue which we have not addressed here. Certainly, since the Euler equations themselves can produce finite-time singularities, it would be surprising if the modified dynamics did not.)

Interestingly, the approach to stratification via modified dynamics may have some physical basis. Vallis *et al.* (1988) have suggested that their modified dynamics mimic, in some ways, the large scales in a turbulent flow. The argument is that, in a turbulent flow, energy is cascaded away to the small scales faster than the invariants of the vorticity field, such as helicity. This leads to coherent, Beltrami-like structures (with $\boldsymbol{\omega} = a\boldsymbol{u}$) in the large scales. This is, of course, just what their dynamics achieve. In the case of swirling or thermally stratified flows, the turbulence energy is, presumably, not only cascaded away, but also transported by internal waves. If the turbulence energy within these waves is removed to the small scales at a rate faster than the vortical invariants, then (37), (38), (43) and (44) may provide a model for the stratification of

angular momentum and temperature in a turbulent flow. (The constant λ would have to be chosen such that $\lambda = \epsilon/\Phi\overline{u_i u_j}$ for swirling flow, or $\lambda = \epsilon/N^2\overline{u_i u_j}$ for buoyancy-driven flow, where ϵ is the dissipation rate of the turbulent kinetic energy.)

We conclude, therefore, that the lower bound on energy in swirling flows ensures that the modified dynamics of Vallis *et al.* will converge to an inviscid stable steady state of arbitrary net azimuthal vorticity. However, the analogy with buoyancy suggests that these are of a degenerate form, corresponding to a stratification of Γ, with a vortex sheet at the boundary. We have been unable to resolve this issue numerically, owing to the development of singularities in the flow field. Nevertheless, if the steady states are indeed of this degenerate form then, perhaps, the modified dynamics can be used to parameterize the stratification of angular momentum and temperature in a turbulent flow.

8. Conclusions

The analogy between swirling and buoyancy-driven flows arises from the way in which vorticity is generated and propagated within each. (The best known illustration of this is internal wave motion.) For a given buoyancy-driven flow, we are often able to construct an analogous swirling flow, as illustrated by the thermal plume structure of figure 1.

The common behaviour of the two flows is reflected in the structure of their steady states. For a small but finite viscosity, these steady flows consist of an inviscid quiescent stratified core, bounded by high-speed wall jets. (The stratification is of Γ or T, depending on the class of flow.) Batchelor regions apart, all of the streamlines pass through both the boundary layers and the core. We may take advantage of this structure to construct an approximate model of these flows, in which the wall jets are handled using a momentum integral technique, and the core and wall flows are matched using continuity of mass. Such models yield reasonable results, accurate to $\sim 10\%$.

The stability of inviscid steady-state flows has been investigated using the energy-minimization technique of Vallis *et al.* The lower bound on the energy of a swirling flow guarantees that stable steady flows do indeed exist. Moreover, these may contain an arbitrary amount of azimuthal vorticity. However, an appeal to the analogous buoyancy-driven flows suggests that these are of a degenerate, stratified form. If this is so, then perhaps the modified dynamics, which disposes of energy while maintaining the vortical invariants, may mimic the evolution towards stratification in a turbulent flow.

The author would like to thank D. Kinnear and Dr C. Marooney for their assistance with the computations, and also a referee for bringing to my attention the work of Pumir & Siggia.

Appendix. Minimum-energy states in swirling flow

Consider an inviscid unsteady swirling flow. Suppose that the fluid is enclosed in a fixed volume V. Then the total kinetic energy for the recirculating flow is

$$E = \int_V \tfrac{1}{2}u_\theta^2 \,\mathrm{d}V + \int_V \tfrac{1}{2}\boldsymbol{u}_p^2 \,\mathrm{d}V = E_\theta + E_p.$$

As a flow evolves, energy may be exchanged between E_θ and E_p, but the total must remain constant. However, for a given flow, conservation of angular momentum imposes a limit on this transfer of energy. Specifically, Schwarz's integral inequality requires

$$E_\theta \geqslant \left\{ \int \Gamma \, \mathrm{d}V \right\}^2 \Big/ 2 \int r^2 \, \mathrm{d}V.$$

The right-hand-side of this expression is fixed by the initial conditions, and consequently we have a lower bound on E_θ. The equality holds if, and only if, $u_\theta = \Omega r$, where Ω is independent of r and z. It follows that rigid-body rotation represents the *absolute* minimum-energy state for a flow with a given net angular momentum. This was noted by Davidson (1989). A related result was shown by Moffatt (1986). He considered the base state $\Gamma = \Gamma_0(r)$ and showed that, for $\Phi > 0$, this represents a *local* minimum in E_θ with respect to a virtual displacement, η, of the Γ-lines. In particular, he found the second-order perturbation in E_θ to be

$$\delta^2 E_\theta = \frac{1}{2} \int_V \Phi(r) \, \eta_r^2 \, \mathrm{d}V.$$

It follows that, as stated above, $\Gamma_0(r)$ is a local minimum in E_θ. Now we know from Rayleigh's stability criterion that $\Gamma_0(r)$ must also represent a local minimum in the total energy $E = E_\theta + E_p$, provided Φ is positive. In fact, we may show that (Davidson 1989)

$$\delta^2 E = \delta^2 E_\theta + \delta^2 E_p = \frac{1}{2} \int_V \Phi(r) \, \eta_r^2 \, \mathrm{d}V + \frac{1}{2} \int_V (\delta^1 \boldsymbol{u}_p)^2 \, \mathrm{d}V,$$

which is consistent with Rayleigh's criteria.

REFERENCES

BATCHELOR, G. K. 1956 On steady laminar flow with closed streamlines at large Reynolds number. *J. Fluid Mech.* **1**, 177–190.

BATCHELOR, G. K. 1967 *An Introduction to Fluid Dynamics*. Cambridge University Press.

DAVIDSON, P. A. 1989 The interaction between swirling and recirculating velocity components in unsteady, inviscid flow. *J. Fluid Mech.* **209**, 35–55.

DAVIDSON, P. A. 1992 Swirling flow in an axisymmetric cavity of arbitrary profile, driven by a rotating magnetic field. *J. Fluid Mech.* **245**, 669–699.

DRAZIN, P. G. & REID, W. H. 1981 *Hydrodynamic Stability*. Cambridge University Press.

ELDER, J. W. 1965 Laminar free convection in a vertical slot. *J. Fluid Mech.* **23**, 77–97.

GILL, A. E. 1966 The boundary layer regime for convection in a rectangular cavity. *J. Fluid Mech.* **26**, 515–536.

GREENSPAN, H. P. 1968 *The Theory of Rotating Fluids*. Cambridge University Press.

JAPAN SOCIETY OF MECHANICAL ENGINEERS 1988 *Visualised Flow*. Pergamon.

KÁRMÁN, T. VON 1921 Uber laminare und turbulente reibung. *Z. Angew. Math. Mech.* **1**, 233–252.

MOFFATT, H. K. 1969 The degree of knottedness in tangled vortex lines. *J. Fluid Mech.* **35**, 117–129.

MOFFATT, H. K. 1985 Magnetostatic equilibrium and analogous Euler flows of arbitrary complex topology. Part 1. Fundamentals. *J. Fluid Mech.* **159**, 359–378.

MOFFATT, H. K. 1986 Magnetostatic equilibrium and analogous Euler flows of arbitrary complex topology. Part 2. Stability considerations. *J. Fluid Mech.* **166**, 359–378.

MOFFATT, H. K. 1988 Generalised vortex rings with and without swirl. *Fluid Dyn. Res.* **3**, 22–30.

PRANDTL, L. 1952 *Essentials of Fluid Dynamics*. Blackie.

PUMIR, A. & SIGGIA, E. D. 1992 Development of singular solutions of the axisymmetric Euler equations. *Phys. Fluids* A **4**, 1472–1491.

SCHLICHTING, H. 1979 *Boundary Layer Theory*. McGraw Hill.

TOWNSEND, A. A. 1976 *The Structure of Turbulence Shear Flow*. Cambridge University Press.

TURNER, J. S. 1973 *Buoyancy Effects in Fluids*. Cambridge University Press.

VALLIS, G. K., CARNEVALE, G. E. & YOUNG, W. R. 1989 Extremal energy properties and constructions of stable solutions of the Euler equations. *J. Fluid Mech.* **207**, 133–152.

VAN DYKE, M. 1982 *An Album of Fluid Motion*. Parabolic.

VIVES, C. & PERRY, C. 1988 Solidification of pure metal in the presence of rotating flows. In *Liquid Metal Flows: Magnetohydrodynamics and Applications* (ed. H. Branover & H. Mond). Progress in Astronautics and Aeronautics, pp. 515–535. AIAA.

VLADIMIROV, V. A. 1985 Example of the equivalence of density stratification and rotation. *Sov. Phys. Dokl.* **30** (9), 748–750.